Received: 15 March 2021 | Revised: 28 September 2021 | Accepted: 20 January 2022

DOI: 10.1002/mp.15510

RESEARCH ARTICLE

MEDICAL PHYSICS

Time-resolved MRI for off-line treatment robustness evaluation in carbon-ion radiotherapy of pancreatic cancer

Giorgia Meschini[1] | **Alessandro Vai**[2] | **Amelia Barcellini**[3] | **Giulia Fontana**[4] | **Silvia Molinelli**[2] | **Edoardo Mastella**[2] | **Andrea Pella**[4] | **Viviana Vitolo**[3] | **Sara Imparato**[5] | **Ester Orlandi**[3] | **Mario Ciocca**[2] | **Guido Baroni**[1,4] | **Chiara Paganelli**[1]

[1] Department of Electronics, Information and Bioengineering, Politecnico di Milano, Milan, Italy

[2] Medical Physics Unit, National Center for Oncological Hadrontherapy (Fondazione CNAO), Pavia, Italy

[3] Clinical Department, National Center for Oncological Hadrontherapy (Fondazione CNAO), Pavia, Italy

[4] Clinical Bioengineering Unit, National Center for Oncological Hadrontherapy (Fondazione CNAO), Pavia, Italy

[5] Radiology Unit, National Center for Oncological Hadrontherapy (Fondazione CNAO), Pavia, Italy

Correspondence
Chiara Paganelli, Department of Electronics, Information and Bioengineering, Politecnico di Milano, Piazza Leonardo da Vinci, 32, 20133 Milan, Italy.
Email: chiara.paganelli@polimi.it

Abstract

Purpose: In this study, we investigate the use of magnetic resonance imaging (MRI) for the clinical evaluation of gating treatment robustness in carbon-ion radiotherapy (CIRT) of pancreatic cancer. Indeed, MRI allows radiation-free repeated scans and fast dynamic sequences for time-resolved (TR) imaging (cine-MRI), providing information on inter- and intra-fraction cycle-to-cycle variations of respiratory motion. MRI can therefore support treatment planning and verification, overcoming the limitations of the current clinical standard, that is, four-dimensional computed tomography (4DCT), which describes an "average" breathing cycle neglecting breathing motion variability.

Methods: We integrated a technique to generate a virtual CT (vCT) from 3D MRI with a method for 3D reconstruction from 2D cine-MRI, to produce TR vCTs for dose recalculations. For eight patients, the method allowed evaluating inter-fraction variations at end-exhale and intra-fraction cycle-to-cycle variability within the gating window in terms of tumor displacement and dose to the target and organs at risk.

Results: The median inter-fraction tumor motion was in the range 3.33–12.16 mm, but the target coverage was robust (-0.4% median $D_{95\%}$ variation). Concerning cycle-to-cycle variations, the gating technique was effective in limiting tumor displacement (1.35 mm median gating motion) and corresponding dose variations (-3.9% median $D_{95\%}$ variation). The larger exposure of organs at risk (duodenum and stomach) was caused by inter-fraction motion, whereas intra-fraction cycle-to-cycle dose variations were limited.

Conclusions: This study proposed a method for the generation of TR vCTs from MRI, which enabled an off-line evaluation of gating treatment robustness and suggested its feasibility to support treatment planning of pancreatic tumors in CIRT.

KEYWORDS
carbon-ion radiotherapy, moving targets, time-resolved MRI

1 | INTRODUCTION

In the past years, particle radiotherapy has attracted increasing interest for the treatment of pancreas cancer, as promising outcomes have been obtained with proton and carbon-ion radiotherapy (CIRT).[1,2] Indeed, particle beams present favorable physical properties, allowing conforming the dose to the target while

sparing surrounding healthy tissues, and offer increased radiobiological effectiveness with respect to X-ray radiotherapy. CIRT is particularly valuable for radioresistant tumors, as the radiobiological effectiveness of carbon-ion beams is independent of the tissue oxygenation rate.[1]

However, pancreas cancer is subject to respiratory motion, which causes target displacement and radiological path length changes, resulting in particle dose distribution variations.[3,4] If not accurately accounted for, these variations can hinder treatment accuracy and efficacy. Different treatment solutions have been proposed, such as (i) breath-holding, (ii) respiratory gating, being the optimal solution in terms of patients' compliance and technical effort, and (iii) tumor tracking, which is not yet clinically implemented in CIRT.[3–5] These techniques are frequently combined with other motion mitigation strategies like abdominal compression and, if pencil beam scanning is adopted, tumor rescanning.[3] In the context of motion management, image-guidance remains an indispensable tool to plan, adapt, and verify the treatment, with computed tomography (CT) and respiratory-correlated (RC) four-dimensional (4D) modality being the current clinical standard.

Nevertheless, RC 4DCT represents a single "average" breathing cycle, which may not be representative of intra- and inter-fraction variability affecting breathing motion.[6] For treatment verification, patients undergo repeated 4DCT scans,[7] thus being exposed to additional non-therapeutic dose. To overcome these limitations, magnetic resonance imaging (MRI) can be considered, as it offers radiation-free acquisitions, improved soft-tissue contrast, and both RC 4D and time-resolved (TR) fast sequences.[8,9] RC 4DMRI can be used to investigate intra- and inter-fraction motion variability,[10–12] by generating virtual 4DCT from repeated 4DMRI for treatment planning and verification.[13–16] TR 3D images still present insufficient spatiotemporal resolution[9]; however, TR 2D cine-MRI can be acquired to describe cycle-to-cycle breathing variations.[17]

To obtain 3D information on breathing organ motion based on 2D cine-MRI, different methods have been proposed in the literature,[18–23] generally relying on a global respiratory motion model[24] which establishes a correlation between a priori knowledge on the breathing motion (e.g., pretreatment 4D imaging) and a surrogate of respiration (e.g., image-based signals[25]). The method by Paganelli et al.,[26] recently validated on both computational and physical phantoms,[21,27] allows TR 3D reconstruction of respiratory motion without the need of previous RC (4D) imaging. Indeed, it relies on 3D motion estimation from 2D deformable vector fields (DVFs) obtained with deformable image registration (DIR) between cine-MRI frames. The method has been demonstrated to outperform approaches based on global motion models, with errors within the imaging data resolution and better performance in the proximity of the intersection between the two orthogonal 2D cine-MRI planes.[21,27]

In this study, we aim at exploiting MRI-guidance for CIRT of pancreas cancer patients, by investigating an approach for the clinical evaluation of gating treatment robustness. Specifically, we integrated the technique of the virtual CT (vCT) from MRI[15,16] with the 3D reconstruction from 2D cine-MRI[26] in order to produce TR vCTs for off-line dose recalculations. We validated the adopted method for the abdominal district on a digital phantom,[28,29] and we performed geometrical and dosimetric quantifications of the impact of breathing motion variability on patients' data for gated CIRT of pancreas cancer.

2 | MATERIALS AND METHODS

2.1 | Dataset

In this study, we considered data from eight pancreas patients treated with CIRT at the Italian National Centre for Oncological Hadrontherapy (CNAO, Pavia, Italy) using the respiratory gating technique.[7,30,31] The study was approved by the local Ethical Committee and informed consent for data acquisition was obtained from the patients according to institutional standards. The motion management strategy at CNAO entails patient immobilization with customized pillows (MOLDCARE Cushion, QFix Avondale PA, USA) and non-perforated body thermoplastic masks (Klarity Medical Products, USA), implying moderate abdominal compression and reduced amplitude of the diaphragm excursion.[32] The same immobilization setup was used for both CT and MRI scans, as well as for treatment delivery.

The 4DCT scans were acquired during free breathing with a Siemens SOMATOM Sensation Open CT (Siemens Healthcare GmbH, Germany) scanner with a resolution of $0.98 \times 0.98 \times 2$ mm. A pressure sensor (AZ-733V system, Anzai Medical Co. Ltd., Japan) placed between the patient's body and the mask provided the external respiratory surrogate signal for 4DCT retrospective reconstruction with phase binning. On the same day of the planning 4DCT (pCT), the patients underwent MRI acquisition on a 3 T scanner (Magnetom Verio, Siemens Healthcare GmbH, Germany). Exploiting the same T2/T1-weighted balanced steady-state free precession sequence (TrueFISP sequence; pixel spacing: 1.33×1.33 mm; slice thickness: 5 mm; repetition time/echo time: 228.07 ms/1.5 ms; accelerating factor: 2; acquisition time: 230 ms), the following dataset was obtained:

1. 4DMRI: multi-slice sagittal images of the abdomen were acquired during free breathing and 4DMRI was retrospectively reconstructed through an algorithm relying on image-based multidimensional surrogates.[10] The imaged volume consisted of 25

sagittal slices, including a field of view (FOV) limited to 12.5 cm in the right–left direction;
2. 2D cine-MRI: two orthogonal (sagittal/coronal) planes intersecting the tumor were acquired in interleaved modality during free breathing for 1.15 min (300 frames in total).

The MRI sequences were optimized to sample the breathing motion while maintaining the total length of the MRI scan acceptable in terms of patient compliance and machine occupation.

Plan setup consisted of two fixed beams, comprising one lateral and one antero-posterior beam ports. Plans were optimized with an intensity-modulated particle therapy (IMPT) algorithm on a 4DCT scan with the RayStation treatment planning system (TPS) (RaySearch Laboratories, Sweden). Patients with pancreatic tumor received a total RBE (Relative Biological Effectiveness)-weighted dose of 57.6 Gy(RBE) in 12 fractions following the institutional protocol. The clinical target volume (CTV) was defined as the gross target volume (GTV) with a 5 mm margin including the locoregional elective lymph nodes and neuroplexus region.[7] The planning target volume (PTV) was then generated by adding 5 mm margin, to account for setup and tumor motion uncertainties.[7] Treatment planning workflow for moving target consisted of plan optimization on the end-exhale pCT and recalculation on the expected gating window phases (i.e., 30%-exhale, 30%-inhale) to evaluate the dosimetric impact of the residual motion.[31] For clinical approval, target dose coverage and organs at risk (OARs) limits must be guaranteed in the three computed dose distributions. However, the proximity of OARs often hinders CTV coverage, and the plan acceptability is then driven by the clinical choice. Therefore, in this study the requested target dose coverage was evaluated on the GTV, entailing that the dose to the 95% of the GTV volume ($D_{95\%}$) was larger than the 95% of the prescription dose. Concerning OARs, the following dose constraints were used in the institutional protocol: for stomach, small bowel, and duodenum, the near-maximum dose ($D_{1\%}$) should be <43 Gy(RBE) and the dose to 5 cc (D_{5cc}) < 36 Gy(RBE); colon $D_{1\%}$ < 48 Gy(RBE), D_{5cc} < 45 Gy(RBE); spinal cord D_{max} < 30 Gy(RBE). Due to the target anatomical position (i.e. pancreas is adjacent to gastrointestinal organs, in particular the duodenum), it may be difficult to define a single-beam geometry that guarantees satisfactory target coverage. In these cases, a mixed prone and supine fractionation scheme was considered by preparing and clinically approving a complete plan for each setup. As MRI data were acquired either in supine (P01–P06) or prone (P07 and P08) setup due to acquisition time constraints, a dedicated plan which satisfied the clinical protocol was prepared for the cases in which the mixed fractionation scheme was adopted for treatment.

2.2 | Time-resolved CT generation

For the generation of TR vCTs from 2D-cine MRI, we followed three main steps (Figure 1): (a) the definition of a reference vCT, corresponding to the reference end-exhale respiratory phase during the MRI scan; (b) the selection of the corresponding reference frames in the 2D cine-MRI dataset; (c) the 3D reconstruction of TR vCTs. The algorithm was implemented in MATLAB (The MathWorks Inc.) and run on a laptop with Intel Core i7-6700HQ CPU at 2.60 GHz, with 16 GB RAM.

2.2.1 | Reference virtual CT

To mimic rigid patient setup in the treatment room at CNAO performed by aligning bones anatomy with X-rays orthogonal projections and/or cone-beam CT images,[33] MR and CT data were rigidly aligned based on the spinal cord before the generation of TR vCTs. Nevertheless, although the 4DCT and MRI scans were performed on the same day, the repositioning of the patient on the MRI scanner couch could cause non-rigid variations in the anatomical configuration of abdominal organs between the CT and the MRI. As such, these differences were considered comparable to inter-fraction motion. It was therefore necessary to generate a vCT (reference vCT) to be used as reference volume to generate TR vCTs.[15] To this aim, the end-exhale MR volume from the 4DMRI was considered. The end-exhale CT from the pCT and end-exhale MR were deformably registered with Bspline DIR (plastimatch.org), thus obtaining a 3D DVF limited to the MR FOV. The DVF was then extended to the FOV of the entire patient anatomy by replicating the motion components at the boundary of the FOV (i.e., in correspondence to the two extreme sagittal slices) to the surrounding voxels.[16] The pCT was therefore deformed according to the resulting DVF to match the abdominal anatomy of the end-exhale MR, yielding the reference vCT (Figure 1a).

2.2.2 | Reference frame selection

To determine the end-exhale phase on the 2D cine-MRI corresponding to the reference vCT, a surrogate was derived from the cine-MRI coronal frames. Optical flow 2D DIR[34] between one randomly chosen frame and all the 150 frames was performed. From the set of 150 2D DVF, the mean motion in the CTV area was extracted, thus obtaining a 1D signal of respiratory motion. All the frames corresponding to the end-exhale respiratory phase were identified on the derived surrogate as local minima. The mean motion among the end-exhale points was computed and the corresponding frame was selected as the reference (Figure 1b).

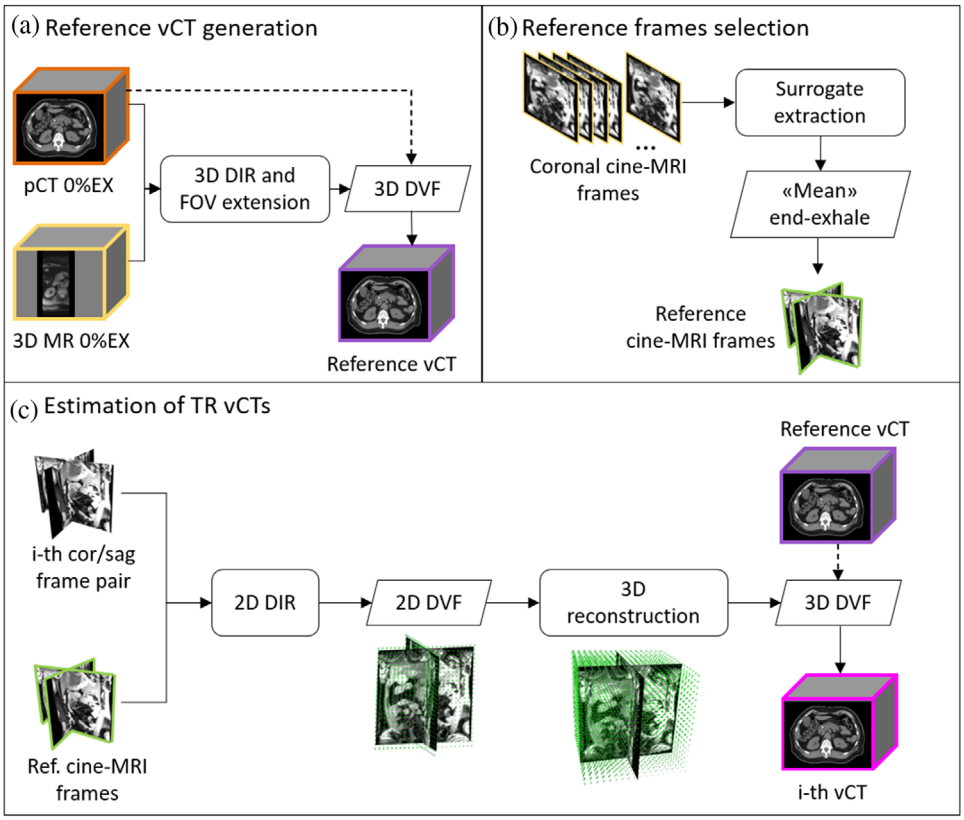

FIGURE 1 Method workflow (a) generation of a reference vCT, (b) selection of the reference frame, (c) derivation of TR vCTs

2.2.3 | DIR and 3D reconstruction

The same optical flow DIR algorithm[34] was used to derive the coronal and sagittal 2D DVF between the selected reference frame and all the other frames. As a result, 150 pairs of coronal/sagittal 2D DVF were obtained. The 3D DVF corresponding to each pair was estimated by propagating to all adjacent planes the right–left and superior–inferior motion components from the coronal DVF, and the antero-posterior information from the sagittal DVF.[26] Due to the abdominal compression applied at CNAO, we assumed negligible motion of the spinal cord and ribs, thus considering the estimated motion only within the lower-thorax and abdomen.[13–16] The reference vCT was finally deformed according to the resulting 3D DVF, thus reconstructing a virtual 3D CT corresponding to each pair of 2D cine-MRI frames (Figure 1c). As a 3D vCT can be estimated for each cine-MRI frame pair, the method gives the possibility to create a TR vCT dataset.

2.3 | Evaluation

The described method was firstly validated on a digital phantom[29,30] (Supporting Information S1, Figures S1 and S2, and Table S1) and then applied on data from eight patients treated at CNAO to evaluate the robustness of clinically acceptable plans for gated CIRT. The target contour was propagated from the pCT to all the vCTs using the estimated 3D DVFs. All contours were then checked and validated by an expert clinician.

2.3.1 | Robustness to inter-fraction variations at end-exhale

The reference end-exhale vCT was used to evaluate inter-fraction target motion by computing the displacement of its center of mass with respect to the end-exhale pCT. The treatment dose was recalculated on the reference vCT. The difference between the recalculated and planned dose distribution was evaluated in terms of dose to the 5% ($D_{5\%}$) and the 95% ($D_{95\%}$) of target volume. Specifically, inter-fraction variations were computed as:

$$\Delta Dx_{\text{inter}} = \frac{D_{x\%}|_{\text{ref vCT}} - D_{x\%}|_{\text{pCT}}}{D_{x\%}|_{\text{pCT}}}$$

where $x = 5$ or 95 (%), and the subscripts "ref vCT" and "pCT" refer to dose computed on reference vCT and planning CT, respectively. The $D_{1\%}$ of relevant OARs (spinal cord, stomach, colon, and duodenum) was also evaluated for the corresponding constraint.

2.3.2 | Robustness to cycle-to-cycle variations within the gating window

The previously described surrogate (Section 2.2.2) was used to identify the end-exhale, end-inhale, and 30%-exhale/30%-inhale respiratory phases, to reconstruct the corresponding TR vCTs. Target displacements between the reference vCT and all the generated vCTs corresponding to the end-exhale phase were evaluated to study end-exhale stability. Similarly, the respiratory phases corresponding to the 30%-exhale and 30%-inhale were obtained, as they represent the extreme respiratory states during gated dose delivery, and used to investigate cycle-to-cycle target motion variability within the gating windows. Target displacements were compared to the maximum motion within the gating window as computed on the 4DCT. To check for significant differences between the motion described by the 4DCT and by the TR vCT dataset, we performed a non-parametric statistical analysis (Wilcoxon signed rank test, $\alpha = 5\%$).

The 25th, 50th, 75th, and 95th percentiles of target displacement as computed on 30%-exhale and 30%-inhale respiratory phases with respect to the reference vCT were identified. Then, the corresponding vCT volumes were used to recalculate the dose. Cycle-to-cycle variations were evaluated as:

$$\Delta Dx_{\text{cycle}} = \frac{D_{x\%}|_{\text{vCT}} - D_{x\%}|_{\text{ref vCT}}}{D_{x\%}|_{\text{ref vCT}}}$$

where $x = 1$, 5, or 95 (%), and the subscripts "vCT" and "ref vCT" refer to dose computed on each vCT and reference vCT, respectively. The $D_{1\%}$ of relevant OARs for each recalculated dose distribution was compared to the respective dose constraint, and to the $D_{1\%}$ corresponding to the reference vCT, to evaluate intra-fraction dose variability.

The differences between inter- and intra-fraction variations were evaluated by comparing the target $D_{95\%}$ and OARs $D_{1\%}$ as obtained from the planned dose, the recalculation on reference vCT, and on gating extreme phases (Friedman test, $\alpha = 5\%$).

3 | RESULTS

3.1 | Robustness to inter-fraction variations at end-exhale

Among all patients, inter-fraction target motion was in median 5.30 mm, ranging from 3.33 to 12.16 mm, and it was mainly in the superior direction (Table 1). Corresponding target $D_{5\%}$ variations were below 1%, whereas $D_{95\%}$ presented a drop up to 16.7% for P05 due to large inter-fraction motion (12.16 mm, Table 2 and Figure 2a,b) while being below 5% for other patients (Table 2, example in Figure 2c,d). The dose to the spinal cord and the colon remained within dose constraints for all patients (Table 2). The $D_{1\%}$ to the stomach was above the constraints for two out of eight patients (P05 and P06), whereas the $D_{1\%}$ of the duodenum was above the constraints for all the eight patients (median $D_{1\%} = 54.3$ Gy(RBE) vs. $D_{1\%} < 43$ Gy(RBE)), as listed in Table 2 (inter-fraction column). The duodenum and stomach $D_{1\%}$ values for all patients are reported in Table S2 of Supplementary materials.

TABLE 1 Inter-fraction target motion, in right–left (RL), antero-posterior (AP), superior–inferior (SI), and three-dimensional (3D)

	RL (mm)	AP (mm)	SI (mm)	3D (mm)
P01	−0.18	−0.09	−5.69	5.69
P02	1.69	−0.32	−2.85	3.33
P03	0.20	0.66	−7.89	7.91
P04	3.50	−3.44	−0.15	4.91
P05	2.19	−3.57	−11.41	12.16
P06	−2.38	−1.66	−2.57	3.88
P07	−1.58	−1.60	−3.69	4.32
P08	−4.25	1.34	−4.68	6.46

3.2 | Robustness to cycle-to-cycle variations within the gating window

The number of reconstructed vCTs varied between 48 (P08) and 96 (P01) (i.e., corresponding to 12 and 24 breathing cycles, respectively). The tumor position at end-exhale was stable (boxplots in Figure S3 of Supplementary materials): the median (interquartile range) value of 3D motion was 1.02 mm (0.64 mm) among all patients. For three out of eight patients (P03, P06, P08), more than 50% of samples at the gating window extreme phases (30%-exhale and 30%-inhale) presented a target motion larger than the maximum gating motion depicted in the 4DCT (Figure 3). Nevertheless, the gating motion among all patients in TR vCTs was in median 1.35 mm, against 1.60 mm in the 4DCTs (no significant difference ($p > 0.05$) was found between the two imaging datasets), and it was generally within 5 mm, that corresponds to the added tumor margins.

Dose changes caused by cycle-to-cycle breathing variability (Table 2, cycle-to-cycle column) resulted in target $D_{95\%}$ variations within ±5%, except for P05, who presented a median 17% dose increase with respect to the dose on the reference vCT. For this patient, the target volume was small (9 cm^3), thus causing the $D_{95\%}$ metric to be very sensitive to motion. Indeed, with a median gating motion below 2 mm (Figure 3a), the $D_{95\%}$ changed from 47.9 Gy(RBE) in the reference vCT to 56.0 Gy(RBE) in the 30%-exhale/30%-inhale vCTs

TABLE 2 Inter-fraction and cycle-to-cycle dose variations to target and organs at risk (OARs)

	Inter-fraction			Cycle-to-cycle			
	Target $\Delta D5_{inter}$	Target $\Delta D95_{inter}$	OARs $D_{1\%}$ > constraint	Target $\Delta D5_{cycle}$	Target $\Delta D95_{cycle}$	OARs $D_{1\%}$ > constraint	OARs $\Delta D1_{cycle}$ > 5%
P01	0.2%	−3.8%	Duod.	0.0%	1.5%	–	–
P02	−0.2%	−0.4%	Duod.	0.0%	−0.3%	Duod.	–
P03	0.2%	−4.4%	Duod.	0.0%	4.1%	Duod.	Stomach
P04	0.1%	0.1%	Duod.	0.0%	0.2%	Duod.	–
P05	0.7%	−16.7%	Duod., stomach	−0.3%	17.0%	Duod., stomach	–
P06	0.1%	0.8%	Duod.	−0.1%	−1.7%	Duod., stomach	Stomach
P07	0.4%	0.9%	Duod.	0.0%	−0.2%	Duod.	–
P08	0.0%	−3.0%	Duod.	0.0%	1.0%	Duod.	Stomach

Note: The columns OARs $D_{1\%}$ > constraint list the relevant OARs whose $D_{1\%}$ exceeds the clinical acceptable threshold. Similarly, OARs $\Delta D1_{cycle}$ > 5% lists the OARs corresponding to median $D_{1\%}$ variation exceeding 5%.
Abbreviation: duod., duodenum.

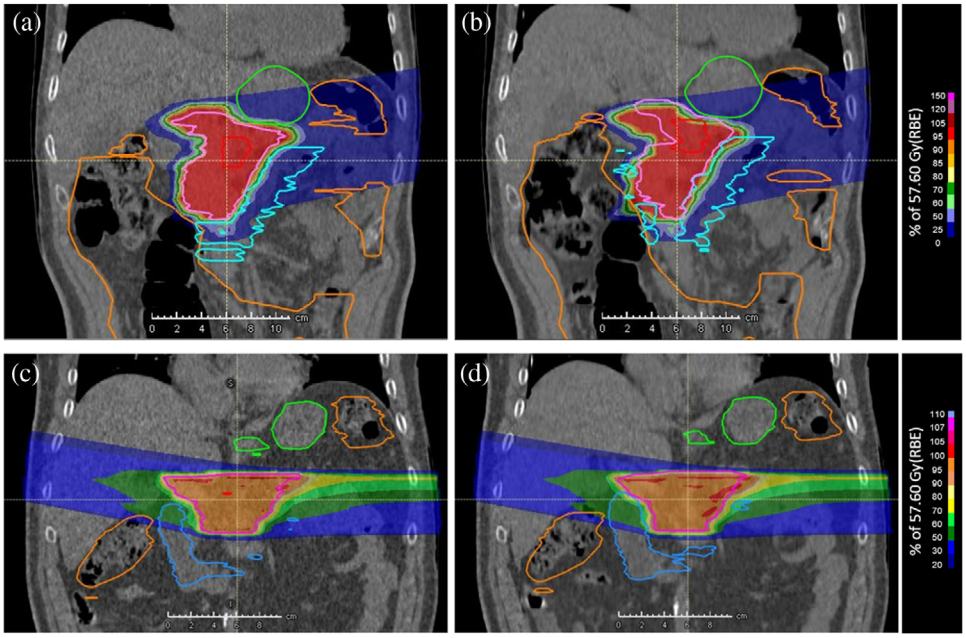

FIGURE 2 Planned dose on end-exhale computed tomography (CT) from the four-dimensional CT (4DCT) (a and c) and recalculated dose on the reference virtual CT (vCT) (b and d) for patients P05 and P01, respectively. The contoured structures represent: gross target volume (GTV) (red), clinical target volume (CTV) (pink), duodenum (light blue), stomach (green), and colon (orange)

(median value). However, in the 30%-exhale/30%-inhale phases the target resulted closer to its planned position, thus producing a partial dose recovery (dose–volume histograms in Figure 4a). The target $D_{5\%}$ variations were below 0.5% for all patients. The $D_{1\%}$ to spinal cord and colon remained below the dose constraints. Differently, in some cases the median $D_{1\%}$ to the stomach and duodenum was above the dose constraints (Table 2). The median (interquartile range) $\Delta D1_{cycle}$ was 0.0% (0.0%) for the spinal cord, -0.9% (1.8%) for the colon, 2.4% (15.9%) for the stomach, and -0.8% (2.4%) for the duodenum. Three patients, whose dose–volume histograms are in Figure 4b–d, presented an increase of $D_{1\%}$ larger than 5% for the stomach (Table 2, see also Supporting Information S2).

As for the comparison between inter- and intra-fraction variations, the target $D_{95\%}$ presented no significant differences between the planned and the recalculated doses (Friedman test, $\alpha = 5\%$). Among OARs, only the duodenum showed significant differences between the $D_{1\%}$ in the planned dose and the dose recomputed on the reference vCT (inter-fraction variation), whereas no significant difference was found between the dose on the reference vCT and the vCT corresponding to extreme phases within the gating window (cycle-to-cycle variations).

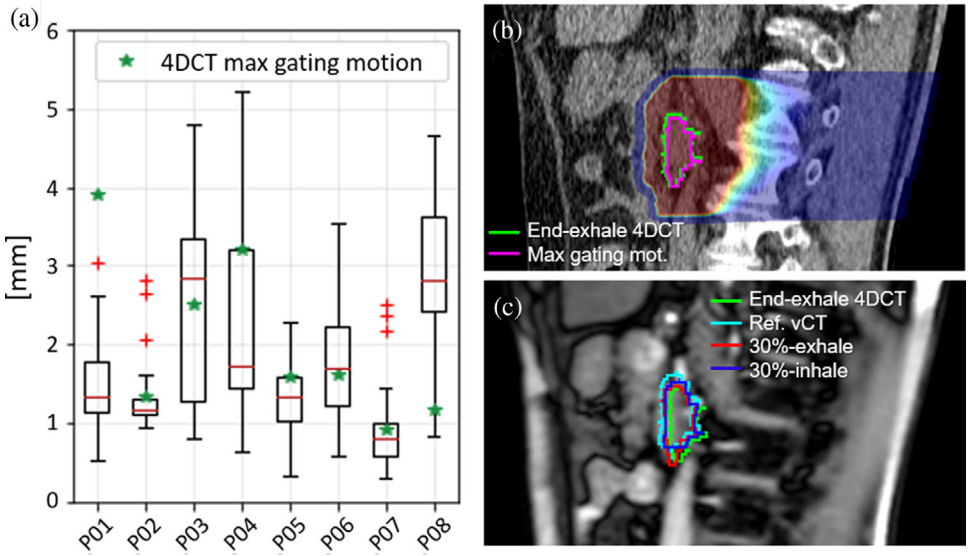

FIGURE 3 Boxplots represent target motion as estimated on 30%-exhale/30%-inhale virtual computed tomographies (vCTs), whereas green stars correspond to the maximum gating motion depicted in the four-dimensional CT (4DCT) (a). For P08, the target contours displaying the maximum gating motion in the 4DCT are represented on the planning CT (b), whereas the contours of the target corresponding to the 95th percentile of gating motion estimated from time-resolved (TR) vCTs are depicted on the reference cine-magnetic resonance imaging (MRI) frame (c)

4 | DISCUSSION

This study investigates a technique to derive TR vCTs from MRI,[16,26] allowing one to evaluate robustness to inter-fraction and cycle-to-cycle breathing variabilities in gated CIRT treatments typically defined on a pCT.

As the method relies on DIR, which is expected to be the main source of uncertainty,[35] we performed a dedicated phantom validation (Figure S2 and Table S1). Considering that the DIR algorithm used for the generation of the reference 3D vCT was demonstrated to have a residual error lower than 2 mm[15] and the optical flow DIR for 2D registration of cine-MRI frames presents sub-voxel precision,[34] our phantom validation confirmed that the method has geometrical accuracy comparable to DIR error and restrained inaccuracy on the dose metrics (≤3.1%).

The comparison between 4DCT and 2D cine-MRI in representing breathing motion was already presented in the literature. Cusumano et al.[36] demonstrated that the 4DCT is sufficient to represent breathing motion for lesions moving less than 7 mm in the superior–inferior direction. Instead, Dhont et al.[6] observed significant intra- and inter-fraction variability for lesions with larger motion amplitudes. Kalantzopoulos et al.[17] studied the respiratory motion of abdominal tumors, highlighting no significant difference during the gating window and significant difference in breathing amplitude (end-inhale to end-exhale) between 4DCT and 2D cine-MRI. Geometric results found in our study were consistent with those by Kalantzopoulos et al., as a significant difference ($p = 0.0078$) was found between motion amplitude in the 4DCT and the 95th percentile of the motion amplitude in the TR vCT dataset derived from 2D cine-MRI (Figures S3 and S4 of Supplementary materials).

By exploiting the derived TR vCTs to evaluate gated treatment plans robustness to inter-fraction variations, our results demonstrated that, despite a median value of 5.30 mm of inter-fraction tumor motion, target coverage was robust (-0.4% median target $\Delta D95_{inter}$). Differently, inter-fraction variations resulted in increased exposure of the duodenum and the stomach. In the clinic, large doses to gastro-intestinal OARs are subject to clinical evaluation and may lead to reoptimization of the dose distribution. It must be noticed that the clinical protocol to treat pancreas cancer provides the use of posterior beams delivered in prone patient positioning to reduce the dose burden to gastro-intestinal organs. In this study, however, imaging data for six out of eight patients were available only in supine positioning, and posterior beams have not been evaluated. The dose increment to OAR, therefore, may be mitigated by considering both prone and supine patient setups. Additionally, as anatomical variations comparable to inter-fraction variations were observed between 4DCT and 4DMRI acquired at the same day, we should mention that future investigations could be focused on the use of repeated 4DMRI to investigate the effect of long-term inter-fraction variations which could more severely affect plan robustness.

Concerning cycle-to-cycle variations, the gating technique resulted effective in limiting tumor displacement during irradiation (1.35 mm median gating motion) and corresponding dose variations (-3.9% median target

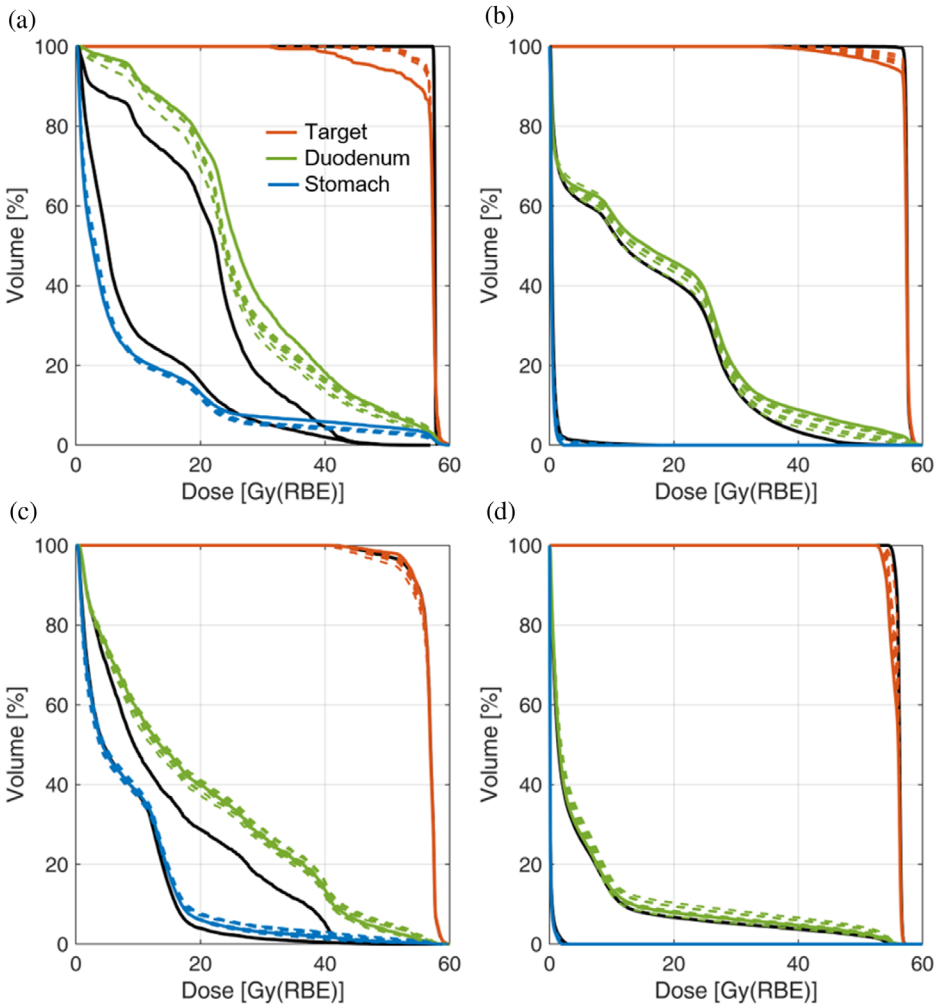

FIGURE 4 Dose–volume histograms of patients P05 (a), P03 (b), P06 (c), and P08 (d). Black curves correspond to the planning computed tomography (CT), solid-colored curves to the reference virtual CT (vCT), and dashed curves correspond to 30-exhale/30-inhale vCTs

$\Delta D95_{cycle}$). This is in accordance with the results of a recent comparative study for proton treatment of pancreatic cancer,[14] in which gating between the 30%-exhale and 30%-inhale phases was demonstrated to outperform gating strategies based on fixed threshold amplitudes or overlap criteria. Although in the TR vCT dataset the dose to the duodenum and the stomach was often above the clinically acceptable threshold, the variations of $D_{1\%}$ with respect to the dose recomputed on the reference vCT were generally low and not statistically significant. This highlights the larger contribution to the dose degradation of inter-fraction rather than cycle-to-cycle variations. The impact of inter-fraction variations was particularly evident for patient P05, exhibiting the largest tumor displacement (12.16 mm), corresponding to a high $D_{95\%}$ drop (16.7%), but also presenting large cycle-to-cycle variations due to the small target volume (Figure 2).

Overall, our work demonstrated the robustness of gated CIRT in pancreas tumors and suggests the use of TR vCTs derived from MRI to support treatment planning. We indeed plan to adopt the TR vCTs to better describe target motion for the selection of the proper motion compensation strategy and to evaluate additional uncertainties scenarios during robust optimization of the treatment plan.[37–40] In perspective, the proposed approach could be also replicated to perform 4D dose optimization[41,42] and dose accumulation,[43,44] as well as it could be integrated with dose variation models[45,46] to explicitly take into account TR 3D deformations. The approximate time required to estimate the vCTs used for dose recalculation was 40 min; this is reasonable for off-line evaluations, but improvements in the implementation could speed up TR vCTs generation. In future works the method could be integrated in the TPS for more efficient generation and use of the TR vCTs.

It should be noted that a limited number of patients was considered in this study, and either supine or prone MRI scans were available. We therefore plan to acquire additional repeated MRI data both in supine and prone

position, to evaluate the clinically delivered dose distributions on a larger patient population. Nevertheless, different patients' characteristics (e.g., tumor positioning with respect to OARs, cycle-to-cycle variability, etc.) might affect the robustness of the treatment plan. As such, the application of the proposed method on a patient-specific basis is suggested to accurately study the impact of inter-fraction variations and respiratory motion variability on CIRT treatments.

5 | CONCLUSIONS

In this study, we exploited TR MRI to evaluate off-line the robustness of gated CIRT treatments of pancreatic cancer. We generated TR vCTs aiming at quantifying inter-fraction and cycle-to-cycle variations to evaluate target coverage and OARs exposure. The results on the considered patient group demonstrated gating treatment robustness and suggested that the proposed method can further support treatment planning and verification for pancreatic tumors in CIRT.

ACKNOWLEDGMENTS

The authors would like to thank Alice Mancin and Luca Anemoni (CNAO, Pavia) for their valuable contribution to data acquisition and patient management. Open Access Funding provided by Politecnico di Milano within the CRUI-CARE Agreement. WOA Institution: Politecnico di Milano.

CONFLICT OF INTEREST

The authors have no conflicts to disclose.

FUNDING INFORMATION

The work was not supported by any funding

DATA AVAILABILITY STATEMENT

Data are available on request due to privacy/ethical restrictions.

REFERENCES

1. Liermann J, Shinoto M, Syed M, Debus J, Herfarth K, Naumann P. Carbon ion radiotherapy in pancreatic cancer: a review of clinical data. *Radiother Oncol*. 2020;147:145.
2. Ng S, Herman J. Stereotactic radiotherapy and particle therapy for pancreatic cancer. *Cancers*. 2018;10:75.
3. Bert C, Durante M. Motion in radiotherapy: particle therapy. *Phys Med Biol*. 2011;56:R113.
4. Mori S, Knopf A, Umegaki K. Motion management in particle therapy. *Med Phys*. 2018;45(11):e994.
5. Riboldi M, Orecchia R, Baroni G. Real-time tumour tracking in particle therapy: technological developments and future perspectives. *Lancet Oncol*. 2012;13:e383.
6. Dhont J, Vandemeulebroucke J, Burghelea M, et al. The long- and short-term variability of breathing induced tumor motion in lung and liver over the course of a radiotherapy treatment. *Radiother Oncol*. 2017;126:339. https://doi.org/10.1016/j.radonc.2017.09.001
7. Vitolo V, Cobianchi L, Brugnatelli S, et al. Preoperative chemotherapy and carbon ions therapy for treatment of resectable and borderline resectable pancreatic adenocarcinoma: a prospective, phase II, multicentre, single-arm study. *BMC Cancer*. 2019;19:922. https://doi.org/10.1186/s12885-019-6108-0
8. Li G, Liu Y, Nie X. Respiratory-correlated (RC) vs. time-resolved (TR) four-dimensional magnetic resonance imaging (4DMRI) for radiotherapy of thoracic and abdominal cancer. *Front Oncol*. 2019;9:1024. https://doi.org/10.3389/fonc.2019.01024
9. Paganelli C, Whelan B, Peroni M, et al. MRI-guidance for motion management in external beam radiotherapy: current status and future challenges. *Phys Med Biol*. 2018;63:22TR03. https://doi.org/10.1088/1361-6560/aaebcf
10. Meschini G, Paganelli C, Gianoli C, et al. A clustering approach to 4D MRI retrospective sorting for the investigation of different surrogates. *Phys Med*. 2019;58:107. https://doi.org/10.1016/j.ejmp.2019.02.003
11. Paganelli C, Kipritidis J, Lee D, Baroni G, Keall P, Riboldi M. Image-based retrospective 4D MRI in external beam radiotherapy: a comparative study with a digital phantom. *Med Phys*. 2018;45(7):3161-3172.
12. Rabe M, Thieke C, Düsberg M, et al. Real-time 4DMRI-based internal target volume definition for moving lung tumors. *Med Phys*. 2020;47:1431.
13. Boye D, Lomax A, Knopf A. Mapping motion from 4D-MRI to 3D-CT for use in 4D dose calculations: a technical feasibility study. *Med Phys*. 2013;40:061702.
14. Dolde K, Naumann P, Dávid C, et al. Comparing the effectiveness and efficiency of various gating approaches for PBS proton therapy of pancreatic cancer using 4D-MRI datasets. *Phys Med Biol*. 2019;64:085011.
15. Meschini G, Vai A, Paganelli C, et al. Virtual 4DCT from 4DMRI for the management of respiratory motion in carbon ion therapy of abdominal tumors. *Med Phys*. 2019;47(3):909.
16. Meschini G, Vai A, Paganelli C, et al. Investigating the use of virtual 4DCT from 4DMRI in gated carbon ion radiation therapy of abdominal tumors. *Z Med Phys*. 2020;S0939-3889(20):30095-30097. https://doi.org/10.1016/j.zemedi.2020.08.005
17. Kalantzopoulos C, Meschini G, Paganelli C, et al. Organ motion quantification and margins evaluation in carbon ion therapy of abdominal lesions. *Phys Med*. 2020;75:33-39.
18. Bjerre T, Crijns S, af Rosenschöld PM, et al. Three-dimensional MRI-linac intra-fraction guidance using multiple orthogonal cine-MRI planes. *Phys Med Biol*. 2013;58:4943-4950.
19. Garau N, Via R, Meschini G, et al. A ROI-based global motion model established on 4DCT and 2D cine-MRI data for MRI-guidance in radiation therapy. *Phys Med Biol*. 2019;64:045002. https://doi.org/10.1088/1361-6560/aafcec
20. Nie X, Rimner A, Li G. Feasibility of MR-guided radiotherapy using beam-eye-view 2D-cine with tumor-volume projection. *Phys Biol Med*. 2021;66:045020.
21. Paganelli C, Portoso S, Garau N, et al. Time-resolved volumetric MRI in MRI-guided radiotherapy: an in-silico comparative analysis. *Phys Med Biol*. 2019;64(18):185013. https://doi.org/10.1088/1361-6560/ab33e5
22. Seregni M, Paganelli C, Lee D, et al. Motion prediction in MRI-guided radiotherapy based on interleaved orthogonal cine-MRI. *Phys Biol Med*. 2016;61:872-887.
23. Fayad H, Buerger C, Tsoumpas C, Cheze-Le-Rest C, Visvikis D. A generic respiratory motion model based on 4D MRI imaging and 2D image navigators. In: 2012 IEEE Nuclear Science Symposium and Medical Imaging Conference Record, California, USA. IEEE; 2009.
24. McClelland J, Hawkes D, Schaeffter T, King A. Respiratory motion models: a review. *Med Image Anal*. 2013;17:19-42. https://doi.org/10.1016/j.media.2012.09.005
25. Tran E, Eiben B, Wetscherek A, et al. Evaluation of MRI-derived surrogate signals to model respiratory motion. *Biomed Phys Eng*

Express. 2020;6(4):045015. https://doi.org/10.1088/2057-1976/ab944c
26. Paganelli C, Lee D, Kipritidis J, et al. Feasibility study on 3D image reconstruction from 2D orthogonal cine-MRI for MRI-guided radiotherapy. *J Med Imaging Radiat Oncol*. 2018;62:389. https://doi.org/10.1111/1754-9485.12713
27. Rabe M, Paganelli C, Riboldi M, et al. Porcine lung phantom-based validation of estimated 4D-MRI using orthogonal cine imaging for low-field MR-linacs. *Phys Med Biol*. 2020;66(5):055006. https://doi.org/10.1088/1361-6560/abc937
28. Paganelli C, Summers P, Gianoli C, Bellomi M, Baroni G, Riboldi M. A tool for validating MRI-guided strategies: a digital breathing CT-MRI phantom of the abdominal site. *Med Biol Eng Compu*. 2017;55(11):2001. https://doi.org/10.1007/s11517-017-1646-6
29. Segars W, Sturgeon G, Mendonca S, Grimes J, Tsui B. 4D XCAT phantom for multimodality imaging research. *Med Phys*. 2010;37:4902. https://doi.org/10.1118/1.3480985
30. Ciocca M, Mirandola A, Molinelli S, et al. Commissioning of the 4-D treatment delivery system for organ motion management in synchrotron-based scanning ion beams. *Phys Med*. 2016;32(12):1667. https://doi.org/10.1016/j.ejmp.2016.11.107
31. Meschini G, Seregni M, Pella A, et al. Evaluation of residual abdominal tumour motion in carbon ion gated treatments through respiratory motion modelling. *Phys Med*. 2017;34:28. https://doi.org/10.1016/j.ejmp.2017.01.009
32. Fontana G, Riboldi M, Gianoli C, et al. MRI quantification of pancreas motion as a function of patient setup for particle therapy—a preliminary study. *J Appl Clin Med Phys*. 2016;17:60.
33. Fattori G, Riboldi M, Pella A, et al. Image guided particle therapy in CNAO room 2: implementation and clinical validation. *Phys Med*. 2015;31(1):9-15.
34. Zachiu C, Papadakis N, Ries M, Moonen C, de Senneville B. An improved optical flow tracking technique for real-time MR-guided beam therapies in moving organs. *Phys Med Biol*. 2015;60:9003-9029.
35. Paganelli C, Meschini G, Molinelli S, Riboldi M, Baroni G. Patient-specific validation of deformable image registration in radiation therapy: overview and caveats. *Med Phys*. 2018;45(10):e908-e922. https://doi.org/10.1002/mp.13162
36. Cusumano D, Dhont J, Boldrini L, et al. Predicting tumour motion during the whole radiotherapy treatment: a systematic approach for thoracic and abdominal lesions based on real time MR. *Radiother Oncol*. 2018;129:456-462.
37. Fredriksson A, Engwall E, Andersson B. Robust radiation therapy optimization using simulated treatment courses for handling deformable organ motion. *Phys Med Biol*. 2021;66:045010.
38. Wolf M, Anderle K, Durante M, Graeff C. Robust treatment planning with 4D intensity modulated carbon ion therapy for multiple targets in stage IV non-small cell lung cancer. *Phys Biol Med*. 2020;65:215012.
39. Mastella E, Molinelli S, Pella A, et al. 4D strategies for lung tumors treated with hypofractionated scanning proton beam therapy: dosimetric impact and robustness to interplay effects. *Radiother Oncol*. 2020;146:213-220.
40. Mastella E, Mirandola A, Russo S, et al. High-dose hypofractionated pencil beam scanning carbon ion radiotherapy for lung tumors: dosimetric impact of different spot sizes and robustness to interfractional uncertainties. *Phys Med*. 2021;10(85):79-86.
41. den Boer E, Wulff J, Mäder U, et al. Technical note: investigating interplay effects in pencil beam scanning proton therapy with a 4D XCAT phantom within the RayStation treatment planning system. *Med Phys*. 2021;48:1448-1455. https://doi.org/10.1002/mp.14709
42. Graeff C. Motion mitigation in scanned ion beam therapy through 4D optimization. *Phys Med*. 2014;30(5):570-577.
43. Mirzapour S, Mazur T, Harold Li H, Salari E, Sharp G. Technical note: cumulative dose modeling for organ motion management in MRI-guided radiation therapy. *Med Phys*. 2021;48(2):597-604. https://doi.org/10.1002/mp.14500
44. Mejers A, Jakobi A, Stützer K, et al. Log file-based dose reconstruction and accumulation for 4D adaptive pencil beam scanned proton therapy in a clinical treatment planning system: implementation and proof-of-concept. *Med Phys*. 2019;46(3):1140-1149.
45. Meschini G, Kamp F, Hofmaier J, et al. Modeling RBE-weighted dose variations in irregularly moving abdominal targets treated with carbon ion beams. *Med Phys*. 2020;47(7):2768–2778. https://doi.org/10.1002/mp.14135
46. Meschini G, Seregni M, Molinelli S, et al. Validation of a model for physical dose variations in irregularly moving targets treated with carbon ion beams. *Med Phys*. 2019;46:3663-3673. https://doi.org/10.1002/mp.13662

SUPPORTING INFORMATION

Additional supporting information may be found in the online version of the article at the publisher's website.

How to cite this article: Meschini G, Vai A, Barcellini A, et al. Time-resolved MRI for off-line treatment robustness evaluation in carbon-ion radiotherapy of pancreatic cancer. *Med Phys.* 2022;49:2386–2395. https://doi.org/10.1002/mp.15510